AJNR

Characteristic Features of MR Truncation Artifacts

Leo F. Czervionke, Jeanne M. Czervionke, David L. Daniels and Victor M. Haughton

Characteristic Features of MR Truncation Artifacts

Leo F. Czervionke[1]
Jeanne M. Czervionke
David L. Daniels
Victor M. Haughton

Truncation artifacts occur in MR imaging because Fourier transforms are used to process MR signal data. These artifacts may alter the intensity, shape, and anatomic detail of structures in the spine. Ring artifacts (Gibb phenomenon) occurring near highly contrasting interfaces represent but one manifestation of truncation artifacts visible on MR images. We review truncation phenomena by providing graphic and phantom models. Ways in which truncation artifacts alter the MR appearance of the spine are discussed.

We found that truncation phenomena are reduced most effectively by using a 256 × 256 matrix whenever feasible.

Truncation artifacts (Gibb phenomenon) have been described thoroughly in mathematical terms in the physics and engineering literature [1–4]. Certain features and examples of the Gibb phenomenon have been explained in the radiologic literature [5–8]. The concept of the Gibb phenomenon, however, is not generally known to most clinical radiologists. The purpose of this article is to provide a practical explanation of the Gibb phenomenon and discuss its importance in evaluating MR images for radiologists who are not familiar with this topic. The significant features of truncation phenomena relevant to MR imaging include: (1) ring artifacts that parallel high-contrast interfaces, (2) artifactual false widening of edges at these interfaces, and (3) edge enhancement of the interface with distortion of tissues immediately adjacent to the interface. Methods of reducing truncation artifacts are discussed.

Mathematical Description of the Truncation Artifact and Gibb Phenomenon

Truncation artifacts occur as a direct result of using Fourier transforms to reconstruct MR signals into images. MR signals are stored in a data array or matrix in the form of free induction decay (FID) signals or echoes of the FID [9]. Each column of information in the data array has a different frequency imparted by the frequency-encoding gradient, and each row of the data array has a different phase relationship imparted by the phase-encoding gradient. Two successive Fourier transforms (actually inverse Fourier transforms) of the data array are carried out to reconstruct the MR data into images.

By means of Fourier transforms, any object may be represented as a sum of multiple sine or cosine waves, each with a given amplitude and frequency [9, 10]. The Fourier transform method is most accurate in depicting regions where there is a gradual change in signal intensity. The use of Fourier transforms to describe a region where there is an abrupt change in signal intensity results in imprecise representation of the interface and tissues immediately adjacent to the interface. This imprecision is represented on the images by truncation phenomena.

An abrupt change in the signal intensity of a region of tissue can be represented graphically by the "step function" shown in Figure 1A. The vertical line between the zones of high and low signal intensity represents a high-contrast interface on an
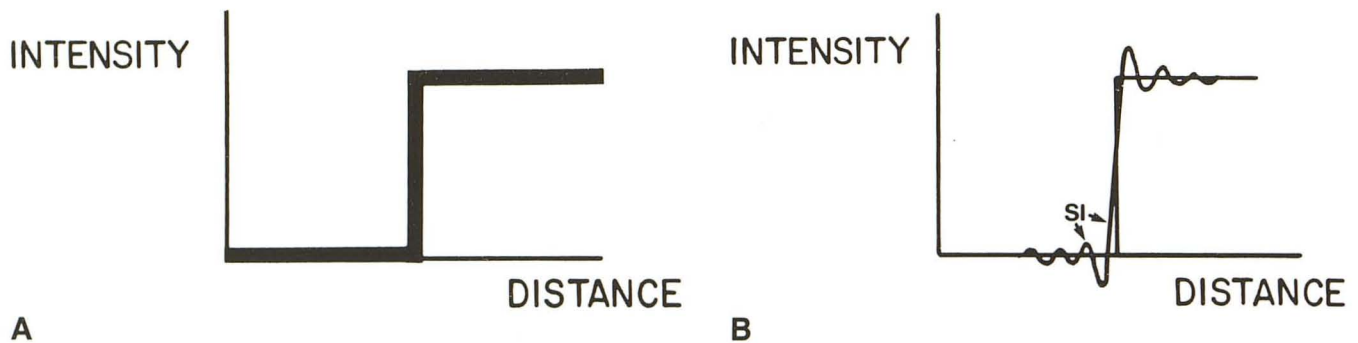
Fig. 1.—*A,* Graphic representation of step function shows abrupt transition in signal intensity. Vertical line between step of high and low signal intensity represents discontinuity in function or interface in image.

B, Step function is shown when Fourier transforms are used to reconstruct image from finite (truncated) data series. Oscillating functions composed of overshoots and undershoots occur on either side of interface and are connected by sloping line passing through interface. The function plotted is a sine integral (SI) function, the oscillating components of which are generated by sinc functions in the reconstruction process. The difference between the sine integral function and the ideal step function is truncation artifact.

MR image. In mathematical terms, this interface is called a discontinuity.

The use of Fourier transforms results in imprecise representation of the discontinuity, which is shown in Figure 1B. In this figure, the step function is present but superimposed on it is another function with peaks and valleys that overshoot and undershoot the intensity of the object on either side of the interface.

A more detailed view of the oscillating function on one side of the interface is seen in Figure 2. Note that the first peak (primary maximum) overshoots the ideal intensity line to a greater degree than successive peaks and valleys do. A similar oscillating function is generated on the low-intensity side of the interface, as seen in Figure 1B. The sum total of the oscillating functions on either side of the interface and the sloping, nearly vertical line passing through the ideal interface is called a sine integral function. This function is the graphic representation of the object and includes truncation artifact. The difference between the ideal step function and the sine integral function shown in Figure 1B is truncation artifact.

Each peak and valley of the sine integral function will correspond to a band of high and low intensity on MR images. The first peak adjacent to the interface always overshoots the ideal intensity line to a greater degree than subsequent peaks do. In similar fashion, the first valley on the low-intensity side of the interface undershoots the ideal intensity line to a greater degree than subsequent valleys do.

The term *Gibb phenomenon* refers to the fact that the initial overshoot on either side of the interface (primary maximum and primary minimum) will persist with an amplitude of 9% of the step function height [5–7], even if an infinite Fourier series is used. Therefore, the Gibb phenomenon can never be completely eliminated even if the data matrix was made infinitely large. In the literature, the concept of Gibb phenomenon has sometimes been broadened to include all fluctuations in signal intensity near a high-contrast interface, but this is not accurate because, in the strict sense, it only refers to the first fluctuation in intensity on either side of the interface [1, 7].

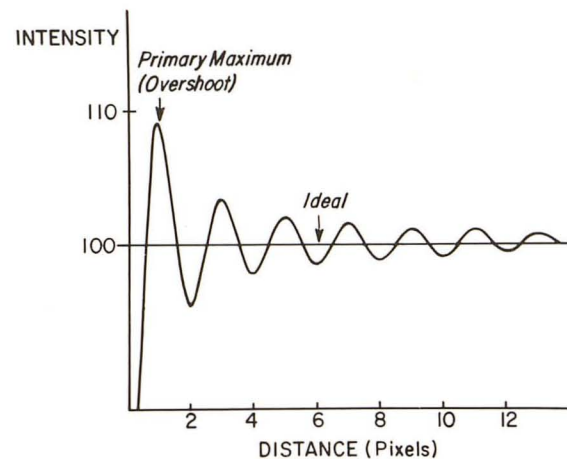The term *truncation artifact* is used because the Fourier

Fig. 2.—Graph of sine integral function generated on high-intensity side of high-contrast interface. The function is oscillating, passing above and below the ideal intensity of the object (step function). The highest peak is called a primary maximum or first overshoot and successive peaks diminish in amplitude with distance from the interface. The first peak overshoots the ideal intensity line by 9%.

series used to reconstruct the signal is not infinite but rather is limited or "truncated" because only a finite amount of data is stored in the matrix (e.g., 128 phase-encoding steps and 256 frequency-encoding steps for a 128 × 256 matrix).

The origin of truncation artifacts in two-dimensional Fourier transformation MR imaging is best understood by using a mathematical approach. The FID signals obtained from a volume of tissue are functions of time. Phase- and frequency-encoding the FID signal effectively converts this function of time into a function of frequency, the components of which are stored in the raw data matrix in rows and columns. The number of frequency (spectral) components stored in the matrix is limited by the size of the image matrix selected.

The truncated data can be written

$$f_t(w) = f(w) \times g(w), \qquad (1)$$

where $f_t(w)$ represents the truncated frequency spectrum and

f(w) is a function representing the potentially infinite number of frequency components contained in the FID. The quantity g(w) is called a "gate" or "window" function [2]. It is a rectangular function of frequency that "recognizes" only frequency components in f(w) that are within a certain range, and discards all others. The frequency range is limited by the sampling frequency. A window function is established in the frequency domain each time the image matrix size is selected. When a larger image matrix is selected, more frequency components contained in f(w) are recognized because the rectangular window is made larger, and the amount of data stored in the matrix will increase accordingly, thereby improving the representation of the object.

The window function g(w) represents the source of truncation artifacts in Fourier transform MR imaging. This can be understood by reconstructing one dimension, for example the "rows" of the data matrix. The Fourier reconstruction of a function f(t) from truncated data is obtained by taking the inverse Fourier transform of equation 1, which results in the formula:

$$f_r^1(t) = f(t) * F^{-1}[g(w)]. \qquad (2)$$

Stated in words, this equation says that the reconstructed function, $f_r(t)$, obtained from truncated data is made of two intertwined (convolved) components: f(t), which is the function describing the precise wave shape and intensity of an object had an infinitely long Fourier series been used, and g(w), the inverse Fourier transform of the window function. A mathematically imprecise but practical way of stating equation 2 is: object appearance in MR image = ideal appearance of object + truncation phenomena.

In equation 2, the inverse Fourier transform of the window function is called a sinc function, and has the form sinc x = (sin π x)/πx, where x in this example is a product of frequency and time (x = wt). This sinc function is an oscillating sinusoidal function and it introduces the fluctuation in signal intensity seen on MR images, near high-contrast interfaces. The sinc function is the mathematical representation of truncation artifact.

However, the position of the truncation artifacts (fluctuations in signal intensity) in the image is not represented precisely by a sinc function, but rather by an integral of the sinc function, the sine integral function [2]. This is because the signal output is expressed in terms of a convolution of two functions of time in equation 2, but this equation cannot be solved in this form. To solve equation 2, it must be rewritten as a so-called convolution integral, which for a step function is given by:

$$f_r(t) = \tfrac{1}{2} + 1/\pi \int_o^x \text{sinc } x \, dx, \qquad (3)$$

where x = wt (i.e., frequency × sampling time). The reconstructed signal is now expressed as a sine integral function. When equation 3 is solved, the result is a distribution of signal intensities at different frequencies. Because the strength of the read-out gradient is known across the object, the spatial

distribution of signal intensities can be plotted for the step function as in Figure 1B.

Analytically, it can be shown that the function in equation 3 changes polarity in the image; that is, crosses the ideal intensity line in Figure 2, whenever the product wt = 1. This happens whenever the frequency (w) of the output signal increases by an amount equal to 1/t, where t = sampling time. In terms of the image this occurs at a distance of every nπ radians (where n = 1,2,3 . . .).

Since the wavelength L of an oscillating function with a constant frequency of oscillation is always a distance of 2π radians, the peaks and valleys (maxima and minima) of the sine integral function always occur at distances from the interface that are multiples of π (Fig. 2). Because pixel diameter (PD) is defined as PD = FOV/N (FOV = field of view, N = matrix size) and L = 2 × PD, then a 1-pixel diameter is a distance of 1π radians from the interface. Therefore, the peaks and valleys of the sine integral function always occur at distances from the interface that are integer multiples of the pixel diameter, regardless of field of view or matrix. It is the pixel diameter that determines the width and spacing of the truncation bands seen on MR images. It is apparent from Figure 2 that each peak or valley is slightly less than 1 pixel in width (measured as the width of each peak at one-half its height). The effect of decreasing pixel diameter is to compress the oscillating function toward the interface (i.e., narrowing the width of each peak and valley thereby crowding them closer together [2]).

Materials and Methods

Truncation phenomena were studied with a computer simulation to display graphically the sine integral function, which is the mathematical function describing object appearance including truncation artifact. The sine integral function was generated for 128 × 256 and 256 × 256 matrices, for one interface and for two interfaces separated by a variable distance. The distance between the interfaces ranged from two to four wavelengths of the sine integral function (the interfaces were separated by 4–8 pixels).

The MR appearance of the truncation artifacts was studied in a phantom made with three test tubes with inner diameters of 6, 8, and 11 mm. The test tubes were filled with normal saline and the tubes were placed in normal saline-containing gelatin. MR scans of this phantom were obtained by using a 1.5-T MR scanner* with spin-echo techniques, 2000/20–80 (TR/TE range), a standard head coil, 128 × 256 and 256 × 256 matrices, 20- and 24-cm fields of view, and 5-mm slice thicknesses.

Results

The plot generated by a sine integral function produced at a single discontinuity interface is seen in Figure 2. Note that the function initially overshoots the intensity of the object by approximately 9%. This is represented by the primary maximum or first peak. The first minimum (valley) is lower in signal intensity than the object. Successive peaks and valleys diminish in amplitude with increasing distance from the interface.

Note that the maximum overshoot (or undershoot) occurs at a distance of precisely ½ pixel from the interface. The first minimum occurs precisely 1 pixel from the interface and so on. The plot shown in Figure 2 is a graphic description of truncation phenomena that occur when Fourier transforms are used to describe a discontinuity. This is well known in the physics and engineering literature [1, 2, 7].

The sine integral functions generated by two boundaries are shown in Figure 3A. When two boundaries of high contrast are separated by 4 pixels, the sinc functions generated by these two boundaries overlap maximally. The function resulting when two sine integral functions are generated and summed together is shown in Figure 3B. Note that the central valley passes beneath the ideal intensity line and two prominent peaks are adjacent to either interface above the ideal intensity line. The implication of this observation is that a prominent band will appear midway between the boundaries, which is lower in intensity than the adjacent tissue. The two peaks above the ideal intensity line on either side of midline indicate that bands of higher signal intensity than that of the actual tissue will occur on either side of the midway point, which distorts the signal intensity of the tissue in this region.

The oscillating function that results when two boundaries are placed farther apart (4.5 pixels) is plotted in Figure 4A. The summation of these two functions is plotted in Figure 4B.

Note that the central valley in this case is wider than that shown in Figure 3B and has diminished amplitude. In a similar fashion, the two peaks located above the ideal intensity line are wider compared with the situation demonstrated in Figure 3A.

When the boundaries are moved 8 pixels apart, the overlapping sine integral functions generated by each boundary (Fig. 5A) produce the summation function plotted in Figure 5B. In this situation there are now four peaks above the ideal intensity line and three valleys below it. However, none of the valleys (minima) have as large an amplitude as that demonstrated in Figure 3B. Therefore, the maximum overlap of the sine integral function, produced by two boundaries, occurs when the distance between the boundaries is precisely 4 pixels.

The phantom study with test tubes of variable diameters illustrated the same features of the Gibb phenomenon as the computer simulation did. On the MR images of the phantom, alternating bands of high and low signal intensity parallel the edges of the test tube. They become less apparent at greater distances from the test tube (Fig. 6). The bands are most conspicuous in the direction of the phase-encoding axis because only 128 phase-encoding samples (views) are obtained in the phase-encoding direction with a 128 × 256 matrix. When the matrix size is changed to 256 × 256, the bands
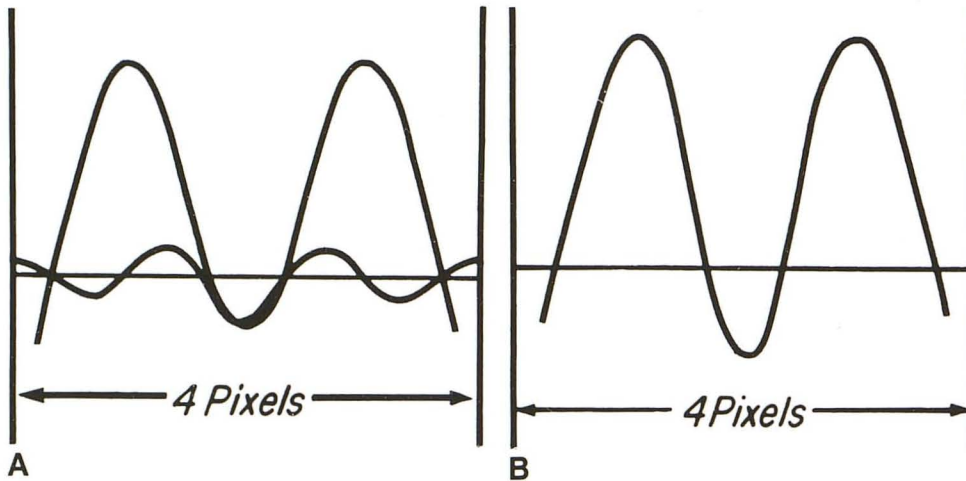

Fig. 3.—Intensity vs distance graphs of two sine integral functions generated by interfaces separated by 4 pixels.

A, Two sine integral functions are generated, one by each interface.

B, The two functions in A are summed and plotted. The valley extending below the ideal intensity line midway between the interfaces corresponds to a midline truncation band. The two peaks on either side of midline cause tissue in this region to have higher signal intensity than ideal tissue would have.
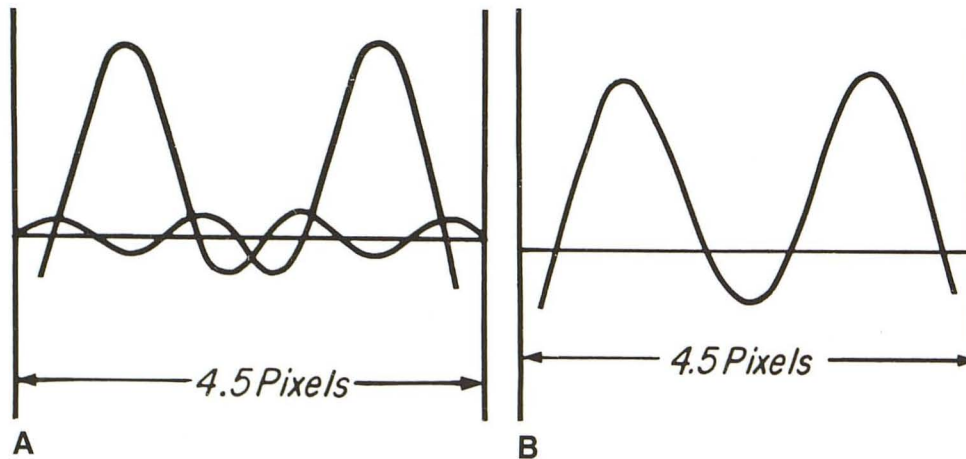
Fig. 4.—Intensity vs distance plots of two sine integral functions generated by interfaces separated by 4.5 pixels.

A, Sine integral functions generated between interfaces are displayed.

B, These functions are summed and plotted. Note that the two peaks above the ideal intensity line and centrally located valley have diminished in amplitude slightly but are wider than those seen in Fig. 3B.
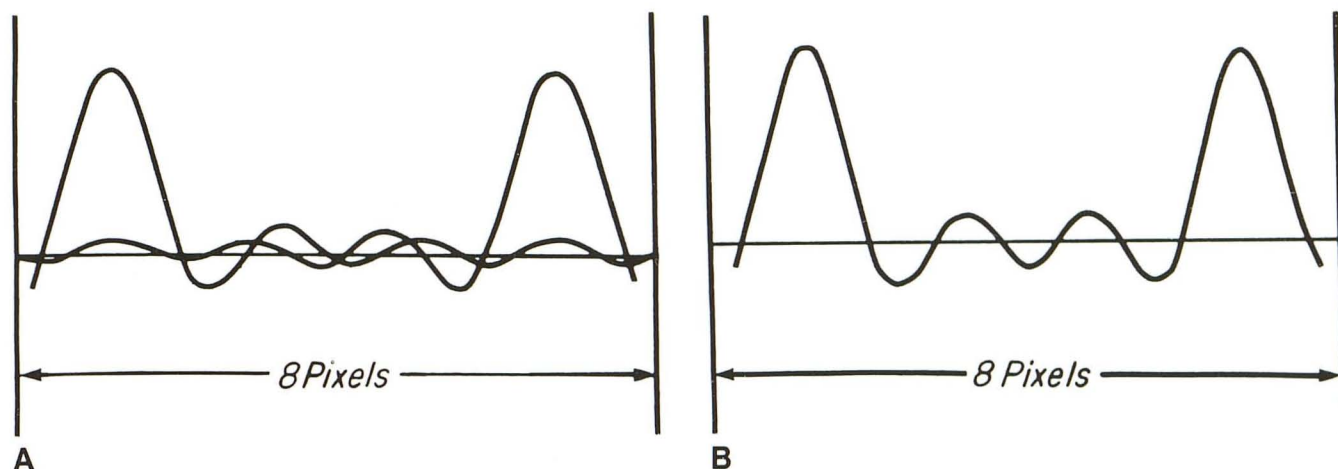
Fig. 5.—Intensity vs distance graphs of sine integral functions generated between interfaces separated by 8 pixels.
A, The two sine integral functions generated are plotted.
B, The summation of the two functions is plotted. At this interboundary spacing, four peaks extend above ideal intensity line and three peaks extend below it; each corresponds to alternating bright and dark truncation bands seen on MR images. The amplitudes of the peaks closest to the interfaces are similar in Figs. 3B, 4B, and 5B. However, the secondary peaks and valleys have progressively decreased in amplitude due to cancellation.
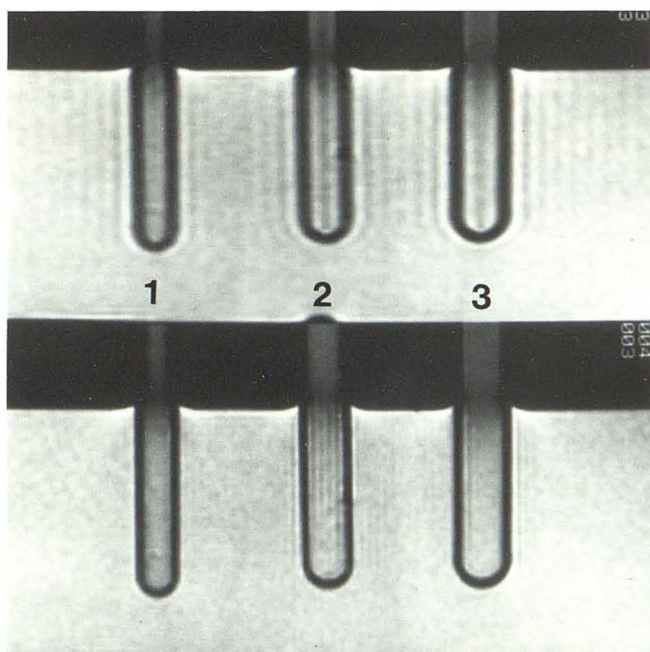

Fig. 6.—Spin-echo images, 2000/20, of test tube phantom. Test tubes 1, 2, and 3 have inner diameters of 6, 8, and 11 mm, respectively.
Top, 128 × 256 matrix with left-to-right phase-encoding axis.
Bottom, 256 × 256 matrix. Truncation bands are less apparent with 256 × 256 matrix. The bands diminished in intensity with increasing distance from the outer margin of the test tubes.

Fig. 7.—Transverse spin-echo images of test tube phantom with phase-encoding axis up and down.
Top, 128 × 256 matrix. Central truncation band has slightly oval configuration and is most pronounced in test tube 2. Diameter of ovoid artifact is greater perpendicular to phase-encoding axis. It is of lower intensity in test tube 3 than in test tube 2. The shape of the test tube wall is distorted along superoinferior phase-encoding axis. Bright truncation ring adjacent to test tube wall imparts edge-enhancing effect.
Bottom, 256 × 256 matrix. Truncation artifacts are symmetric and less conspicuous.

become thinner and less apparent and appear closer to the edges of the test tubes. Also notice that the walls of the test tube appear thinner in the direction of the phase-encoding axis as the phase-encoding steps are increased from 128 to 256.

The effect of altering interboundary spacing is also shown in the test tube phantom (Fig. 6). In the top row, test tube 2
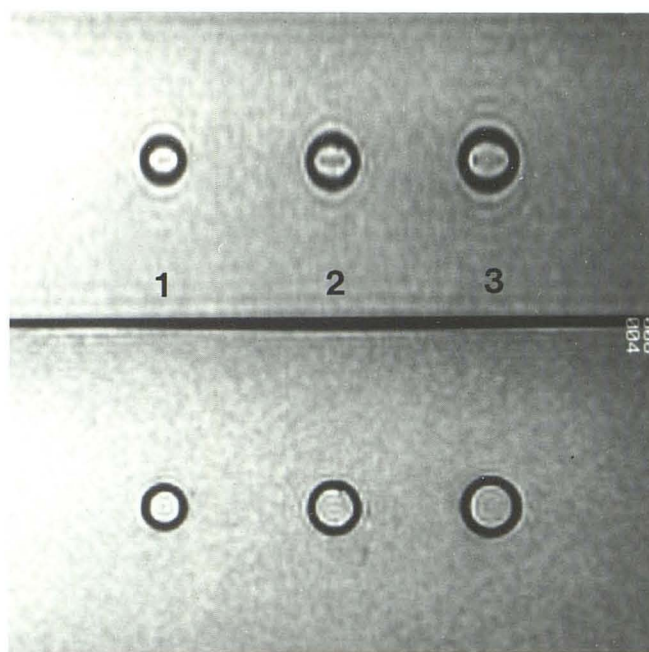
contains a thinner and darker central band than is seen in test tube 3 because the inner diameter of test tube 2 is approximately 7.5 mm, which represents a distance of 4 pixels when a 128 × 256 matrix and 24-cm field of view are used. The change in appearance of the central dark band seen in
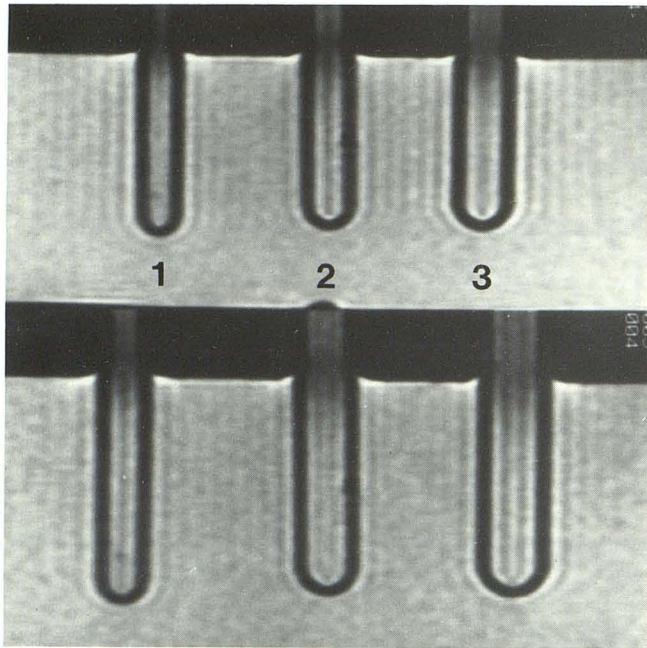
Fig. 8.—MR images 2000/20, of test tube phantom with 24-cm (*top*) and 20-cm (*bottom*) fields of view. Effect of decreasing field of view is to decrease pixel diameter. *Bottom* image has more truncation bands between test tube walls.

test tubes 2 and 3 correlates with the configuration of the central valley seen in the plots shown in Figures 3B and 4B. In other words, the central dark band widens but diminishes in amplitude as the interboundary distance changes from 4 to 4.5 pixels.

With a 256 × 256 matrix, there are several faint alternating low- and high-signal bands within the test tubes (Fig. 6, bottom row, test tube 2). These bands appear thinner and less intense because the pixel diameters have been reduced by one-half by increasing matrix size from 128 × 256 to 256 × 256. Therefore, increasing matrix size has an effect similar to increasing the distance between boundaries from 4 to 8 pixels (Fig. 5).

Figure 7 shows truncation artifacts in the test tube phantom imaged transversely (axial plane). Note that a 128 × 256 matrix results in an asymmetric appearance of the truncation bands or rings. The rings appear more evident in the direction of the phase-encoding axis. The central dark band has an ovoid configuration. In addition, the walls of the test tubes are thicker along the phase-encoding axis (128 steps) compared with the frequency-encoding direction (256 samples). When the matrix size is changed to 256 × 256, the truncation artifacts are less conspicuous and appear symmetrically around and within the test tube. In addition, the wall of the test tube is of uniform thickness with the 256 × 256 matrix.

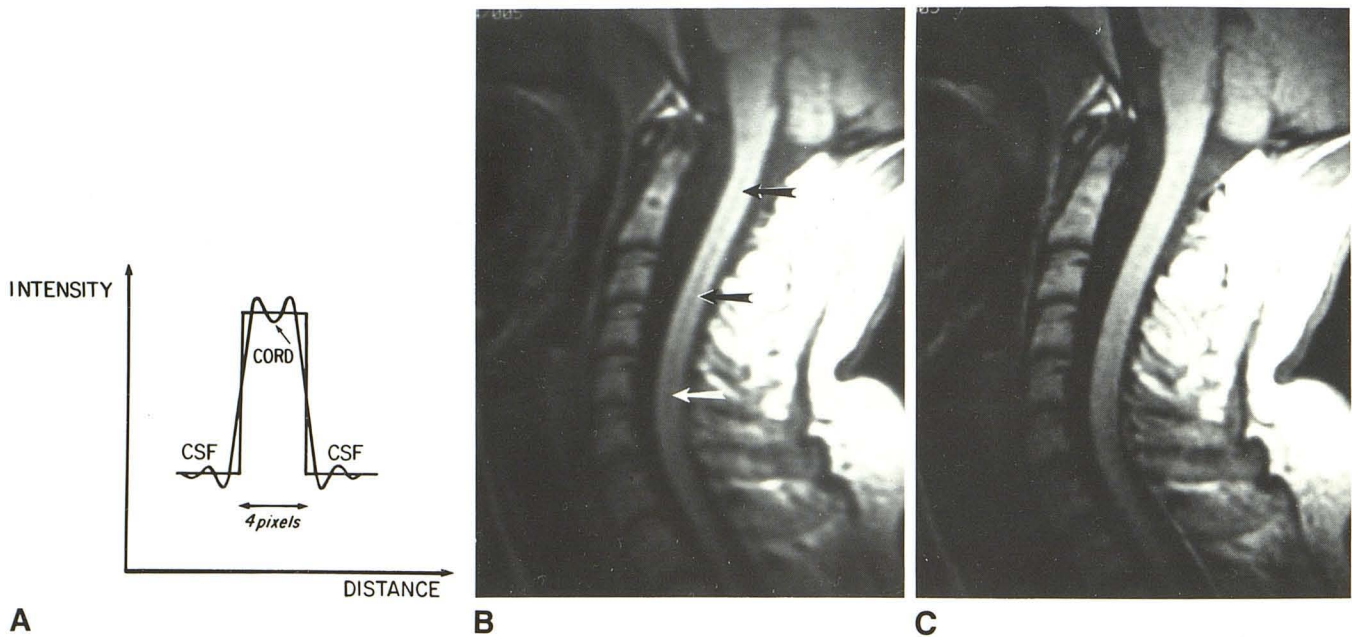The effect of changing the field of view is shown in Figure

Fig. 9.—*A*, Diagram of cord/CSF interface for T1-weighted image where CSF has lower signal intensity than cord. Sine integral functions generated at each interface are shown and reinforce one another between the two interfaces. The small valley (*arrow*) projecting below ideal intensity of cord produces central dark truncation band seen in *B*.
B, Sagittal T1-weighted image of cervical spine with 128 × 256 matrix. Peaks above ideal intensity line make cord appear brighter on either side of central dark band (anteroposterior phase-encoding direction).
C, 256 × 256 matrix. Truncation bands are not apparent. Anteroposterior diameter of cord appears smaller in *B* than in *C*.
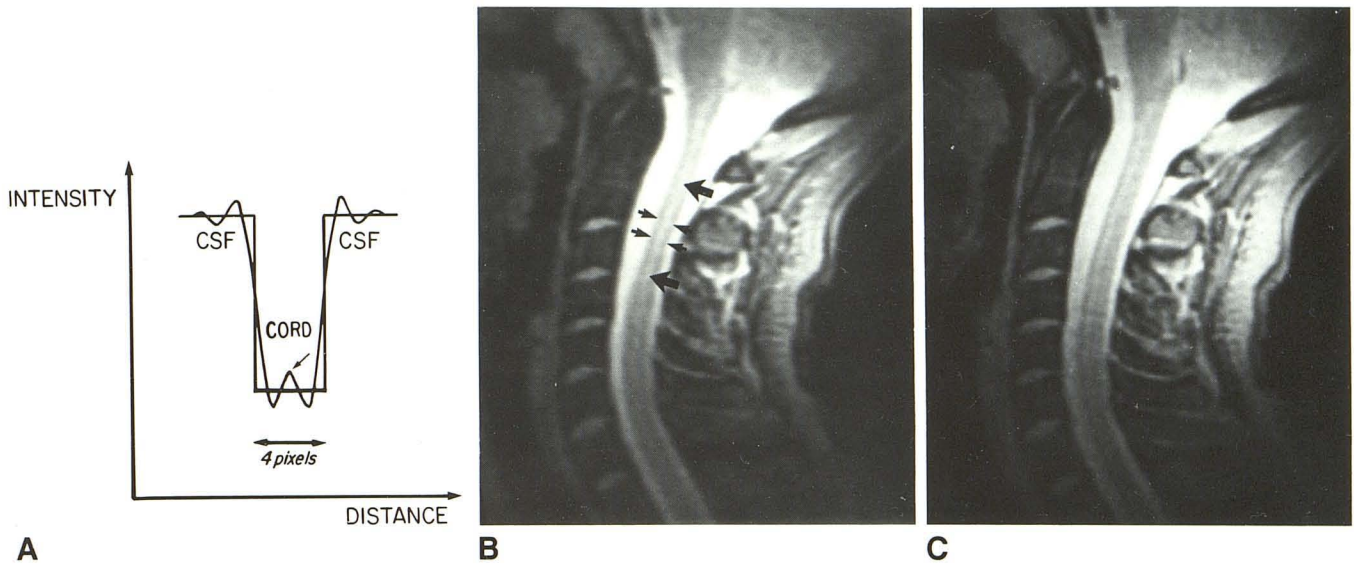
A

B

C

Fig. 10.—*A*, Signal intensities of cord and CSF for T2-weighted image. In this case, overlapping sine integral functions between cord interfaces are reversed when compared with Fig. 9A. A central peak (*arrow*) extends above ideal intensity line of cord, and two valleys are seen on either side of central peak.

B, Sagittal T2-weighted image of cervical spine shows bright, centrally located truncation band (*large arrows*) in cord corresponding to midline peak seen in *A*. Signal intensity of cord (*small arrows*) on either side of this central bright band is darker than it should be because of undershoot on either side of central peak, shown in *A*.

C, Same parameters as *B* except for 256 × 256 matrix. Central bright truncation band disappears, leaving thin strip of high signal intensity in cord anterior to midline representing central gray matter. Anteroposterior diameter of spinal cord appears smaller in *B* than in *C*.

Fig. 11.—Sagittal T1-weighted image, 800/20, of cervical spine obtained with a 24-cm field of view and 128 × 256 matrix with anteroposterior phase-encoding axis in spine. Note dark truncation bands (*arrows*) altering signal intensity of marrow in these vertebral bodies. Also note faint, dark, centrally located truncation band in spinal cord. Incidentally, disk material protrudes into ventral aspect of spinal canal at C3–C4, C4–C5, and C5–C6 levels.
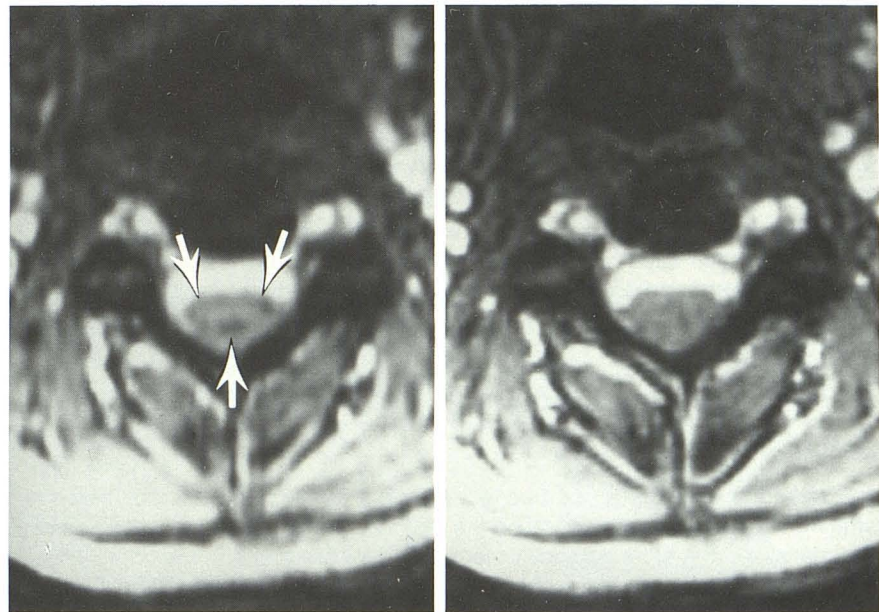
A

B

Fig. 12.—Single-slice gradient-echo images, 100/12, with a 24-cm field of view, 30° flip angle, and up-and-down phase-encoding axis.

A, 128 × 256 matrix. Note bright ovoid truncation artifact in spinal cord. Surrounding this is ring of lower signal intensity (*arrows*) representing initial "undershoot" adjacent to interfaces.

B, 256 × 256 matrix. Artifact is less evident. Anteroposterior diameter of cord in *A* appears smaller than in *B*.
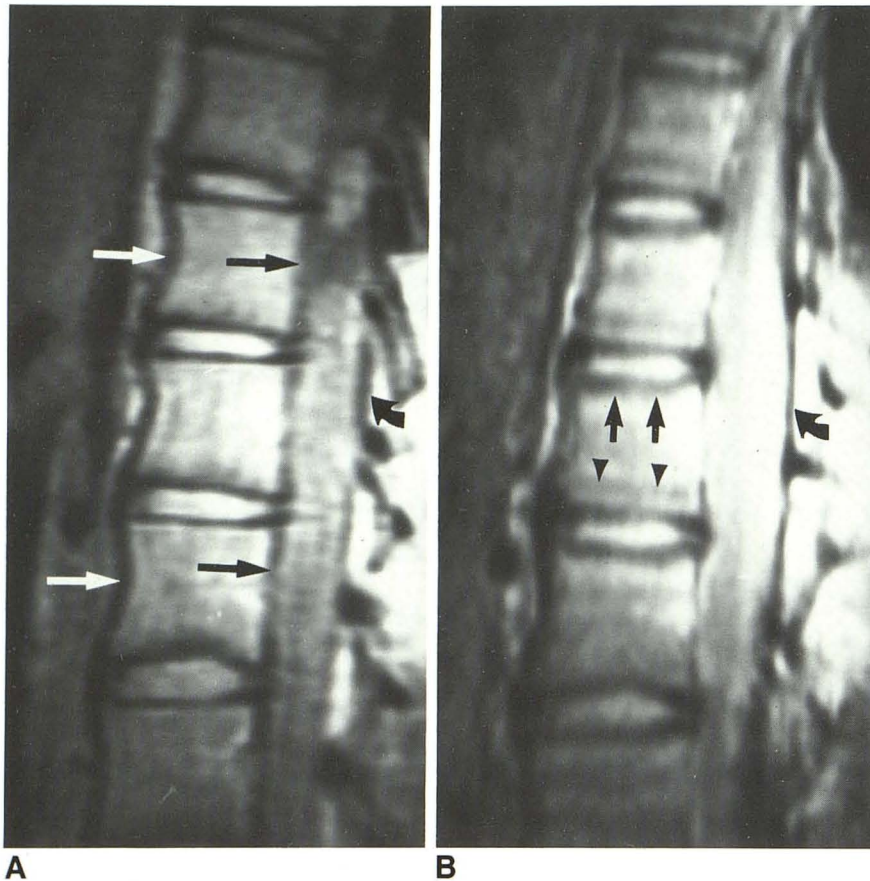
A   **B**

8. Figure 8, top row, was obtained with a 24-cm field of view and is identical to Figure 6, top row. Figure 8, bottom row, was obtained with a 20-cm field of view, the other parameters being identical. Here, test tube 1 contains a prominent dark central truncation band, whereas test tubes 2 and 3 contain several bright and dark truncation bands. Therefore, the effect of decreasing the field of view is the same as increasing the interboundary spacing and is similar to that graphically shown in Figures 3 and 5.

Discussion

A test tube phantom is not a perfect phantom for demonstrating truncation artifacts because the test tube walls have thickness, and therefore both the outer and inner walls of the test tube represent four high-contrast interfaces in proximity. Therefore, the truncation effects produced by these four interfaces are not identical to the situation simulated graphically by the computer. However, the test tubes do illustrate the effect of altering matrix size, field of view, and changing interboundary spacing as predicted by the computer-generated plots.

In reality, MR images depict body tissues composed of many high- and low-contrast interfaces. The sine integral functions generated by these multiple interfaces summate and tend to reinforce or cancel each other to give the overall truncation effect seen on the MR image. The maximum truncation effect occurs midway between two interfaces when

the distance between the interface is precisely 4 pixels (Fig. 3). One example is the highly contrasting interfaces between CSF and spinal cord on T1-weighted cervical spine MR images. When the distance between anterior and posterior margins of the cord is approximately 4 pixels (depending on field of view and matrix size), a midline truncation band is apparent in the cord (Fig. 9). A central truncation band is dark compared with the cord on T1-weighted images because the CSF is dark [11]. This situation is shown schematically in Figure 9A. The sum of the sine integral functions generated by each cord/CSF interface is negative midway between the interfaces and is negative in amplitude relative to the true tissue intensity of the cord. The central truncation band will never be as dark as CSF, however, because the amplitude of the function is never greater than 9% of the signal-intensity difference at the cord/CSF interface. The dark truncation band within the cord on a 128 × 256 matrix may be confused with a syrinx [11]. This truncation band is not apparent when the matrix size is changed to 256 × 256 (Fig. 9C).

The opposite situation is seen whenever the CSF is of higher signal than the cord, such as on a T2-weighted image of the cervical spine (Fig. 10). This situation is shown schematically in Figure 10A. Note that the summated sine integral functions result in a central peak above the real intensity line midway between the cord/CSF interfaces when the distance between the interfaces is 4 pixels. This results in the relatively bright truncation band seen midline in the cord in Figure 10B. This central truncation band should not be confused with the

true central gray matter, which is seen on midsagittal images of the cord as a thin stripe of high signal anterior to cord midline when a 256 × 256 matrix is used (Fig. 10C) [11]. It is obvious from these two examples that the central truncation band between two interfaces always reflects the signal intensity of the tissue outside the interfaces but not to the same degree of intensity. There are other situations in which truncation bands distort the signal intensity of other tissues in the spine such as the intervertebral disk and bone marrow (Fig. 11).

Other features of truncation phenomena relevant to MR imaging have not been stressed in the literature. For example, truncation artifacts impart an edge-enhancing characteristic to any high-contrast interface. This edge-enhancing effect is due to the presence of the first large peak or valley adjacent to the interface. This can be seen schematically in Figure 10A. Note that the summed function dips below the intensity of the cord on either side of the cord midline. This results in an abnormally low signal intensity of the cord between the central bright truncation band seen in Figure 10B and the cord/CSF interface. Similarly, the CSF adjacent to the cord is brighter than in reality because of the overshoot of the sine integral functions seen in Figure 10A. The truncation bands in the CSF, however, may not be apparent depending on the window levels and widths selected. The initial overshoot and undershoot on either side of the interface cannot be eliminated even by increasing the matrix infinitely (refer to the mathematical description of Gibb phenomenon). Therefore, this edge-enhancing feature of truncation phenomena cannot be eliminated completely. Increasing matrix size will diminish the width of the undershoot and overshoot adjacent to the interface and thereby narrow the band of enhancement (compare Figs. 10B and 10C). This edge-enhancing feature of truncation phenomena does not necessarily result in better definition of the interface. In fact, this edge enhancement distorts normal anatomic detail and may alter the apparent size of the object. For example, in Figures 9, 10, and 12, the anteroposterior diameter of the spinal cord appears smaller than normal because the CSF adjacent to the spinal cord margins is brighter than normal, especially when a 128 × 256 matrix is used.

Truncation artifacts may also cause high-contrast interfaces (such as cortical bone edges) to appear thicker than in reality, because the sine integral function has a sloping line that extends through the actual interface (Fig. 1). This sloping line through the interface has a more vertical orientation with increased matrix size and therefore more accurately depicts the actual width of the boundary when the pixel diameter is smaller. False thickening and blurring of edges are seen readily adjacent to cortical bone such as vertebral body margins, vertebral endplates, ligaments, and margins of the dural sac (Figs. 13 and 14).

Minimizing Truncation Artifacts in MR Imaging

Ways of minimizing truncation artifacts have been described [5, 6]. One method is decreasing pixel diameter, which can be accomplished either by increasing matrix size or by decreasing the field of view. With smaller pixel diameters edge detail is more accurately demonstrated on MR images (Fig. 14) and the truncation bands are less obvious. However, increasing the matrix size has the same effect as increasing the distance between two interfaces; that is, multiple truncation artifacts are seen between the boundaries but the intensity and width of the truncation bands diminish (Figs. 5 and 6). If the data matrix could be made infinitely large, all secondary peaks and valleys would cancel each other completely. However, the initial overshoot (or undershoot) of the sine integral function on either side of the interface always persists. Gibb phenomenon can never be completely eliminated even with an infinite Fourier series [1, 7].

Another method of minimizing the effects of truncation artifacts is to filter the raw data. In the literature, this is sometimes called *apodization* [12, 13]. The raw data are collected and stored in the frequency domain. A mathematical filter, which is a function of frequency, is applied to the raw data to remove high-frequency information. Examples of such high-frequency filters go by such names as "Hamming window," "Hanning window," or "triangular window." These high-
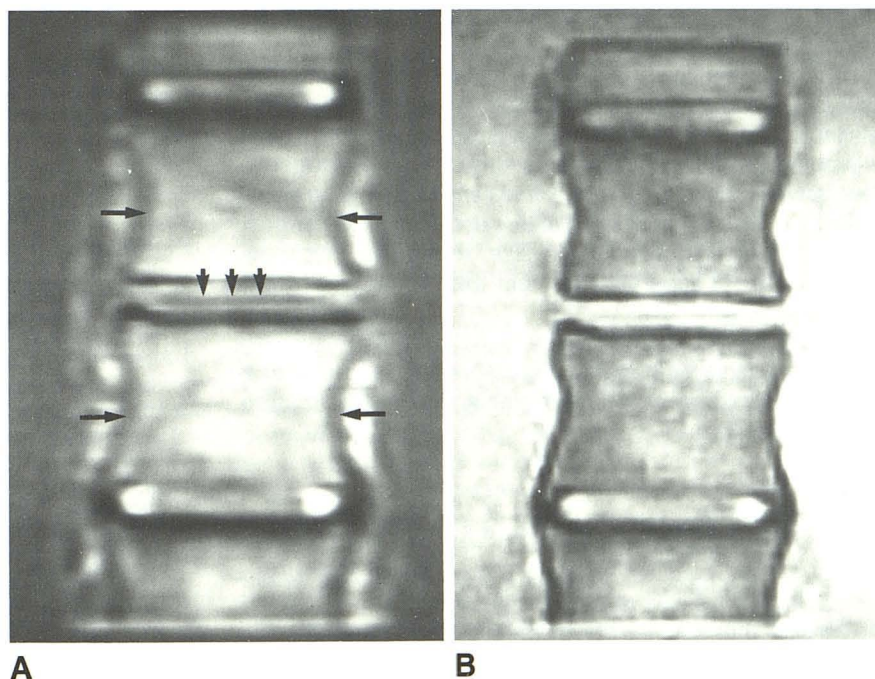

Fig. 14.—Coronal images, 800/20, of vertebral body phantom. Centrally located intervertebral disk was removed and phantom immersed in bath of saline and copper sulfate. Image parameters were 20-cm field of view, right-to-left phase-encoding axis, and 128 × 256 (*A*) and 256 × 256 (*B*) matrices. Lateral cortical margins (*long arrows*) of vertebral bodies are thicker in *A* than in *B*. However, thickness of vertebral endplates is the same in *A* and *B*. Note centrally located truncation artifact in mid intervertebral disk space (*short arrows*).
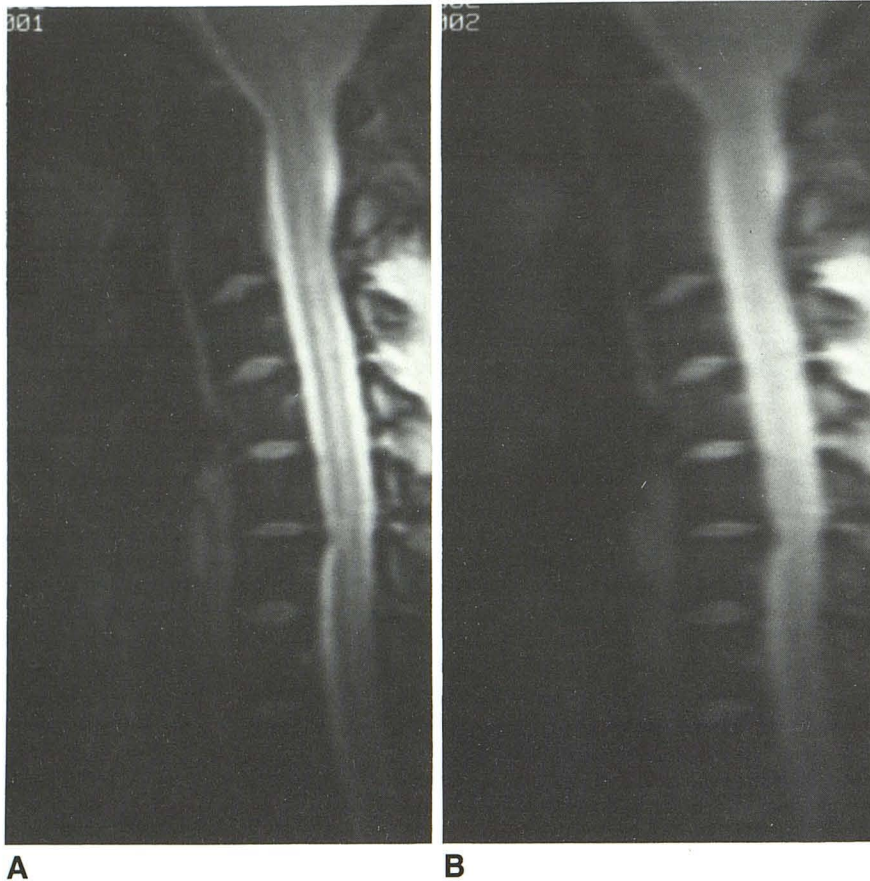
A

B

A **B**

Fig. 15.—Effect of filtering on MR imaging. Sagittal images, 2000/20, of cervical spine with 256 × 256 matrix and cardiac gating.
A, Unfiltered.
B, After filtering raw data with a Hanning window. Loss of spatial resolution results in image blurring.

frequency filters either eliminate or partially eliminate the secondary maxima and minima of the sine integral function. However, filtering often does not eliminate the primary overshoot and undershoot. In fact, the width of the first peak may be increased by filtering [12, 13]; in addition, filtering results in a more gradual slope of the sine integral function through the interface, and this results in a loss of spatial resolution; that is, image blurring (Figs. 15 and 16). Filtering has uses in Fourier spectroscopy but because of image blurring is not practical for MR imaging.

Truncation artifacts may also be reduced by altering window levels and window widths. The visualization of certain tissues of interest may be affected as well.

In summary, truncation artifacts may distort MR images in several ways, including (1) artifactual bands altering the signal intensity of tissue, (2) blurring and widening of high-contrast interfaces, (3) distortion of the size and shape of certain objects, and (4) edge enhancement and distortion of high-contrast interfaces.

The effects of truncation phenomena are most effectively reduced by increasing matrix size. Therefore, the use of a 256 × 256 or larger matrix is recommended for MR imaging whenever feasible.
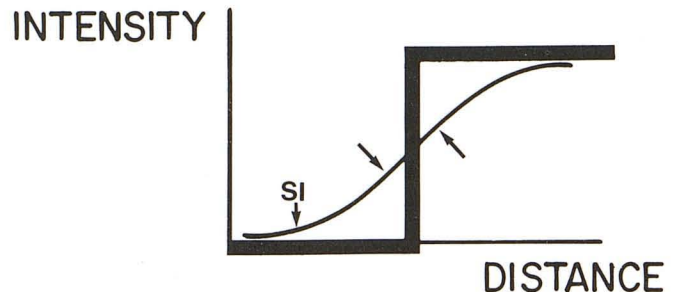

Fig. 16.—Effect of filtering on sine integral (SI) function. By using a triangular window, oscillatory components of sine integral function are removed (compare with Fig. 1B), but sloping line (*arrows*) through interface poorly approximates discontinuity of ideal step function, resulting in image blurring.

REFERENCES

1. Carslaw HS. *An introduction to the theory of Fourier series and integrals.* New York: Dover, **1950**
2. McGillem CD, Cooper GR. *Continuous and discrete signal and systems analysis.* New York: Holt, Rinehart and Winston, **1974**
3. Castleman KR. *Digital image processing.* Englewood Cliffs, NJ: Prentice-Hall, **1979**
4. Bracewell RN. *The Fourier transform and its applications.* New York: McGraw-Hill, **1978**
5. Wood ML, Henkelman RM. Truncation artifacts in magnetic resonance imaging. *Magn Reson Med* **1985**;2:517–526
6. Lufkin RB, Pusey E, Start DD, Brown R, Leikind B, Hanafee WN. Boundary artifact due to truncation errors in MR imaging. *AJR* **1986**;147:1283–1287
7. Schenck JF, Hart HR, Foster TH, Edelstein WA, Hussain MA. High resolution magnetic resonance imaging using surface coils. In: Kressel HY, ed. *Magnetic resonance annual 1986.* New York: Raven, **1986**:150–152
8. Daniels DL, Czervionke CF, Breger RK, et al. "Truncation" artifact in MR images of the internal auditory canal. *AJNR* **1987**;8:793–794
9. Wehrli FW, MacFall JR, Newton TH. Parameters determining the appearance of NMR images. In: Newton TH, Potts DG, eds. *Advanced imaging techniques.* San Anselmo, CA: Clavadel, **1983**:81–117
10. Pykett IL. NMR imaging in medicine. *Sci Am* **1982**;246:78–88
11. Czervionke LF, Daniels DL, Ho PSP, et al. The MR appearance of gray and white matter in the cervical spinal cord. *AJNR* **1988**;9:557–562
12. Norton RH, Beer R. New apodizing functions for Fourier spectrometry. *J Opt Soc Am* **1976**;66:259–264
13. McVeigh ER, Henkelman RM, Brouskill MJ. Noise and filtration in magnetic resonance imaging. *Med Phys* **1985**;122:586–591